CENTER FOR CONNECTED AND AUTOMATED TRANSPORTATION

Final Report #ICT-21-039
November 2021

# Passive Sensing of Electromagnetic Signature of Roadway Material for Lateral Positioning of Vehicle

Jeffery R. Roesler
*Professor & Associate Head*

Sachindra Dahal
*Graduate Research Assistant*

ILLINOIS CENTER FOR TRANSPORTATION

# DISCLAIMER

Funding for this research was provided by the Center for Connected and Automated Transportation under Grant No. 69A3551747105 of the U.S. Department of Transportation, Office of the Assistant Secretary for Research and Technology (OST-R), University Transportation Centers Program. The contents of this report reflect the views of the authors, who are responsible for the facts and the accuracy of the information presented herein. This document is disseminated under the sponsorship of the Department of Transportation, University Transportation Centers Program, in the interest of information exchange. The U.S. Government assumes no liability for the contents or use thereof.

## Suggested APA Format Citation:

Dahal, S., & Roesler, J. R. (2021). *Passive sensing of electromagnetic signature of roadway material for lateral positioning of vehicle* (Report No. ICT-21-039). Illinois Center for Transportation. https://doi.org/10.36501/0197-9191/21-039

## Contacts

For more information:

Sachindra Dahal
University of Illinois at Urbana–Champaign
B235 Newmark Civil Engineering Laboratory
205 North Mathews Avenue, Urbana, IL 61801
sdahal2@illinois.edu
(217) 300-1488
https://ict.illinois.edu

CCAT
University of Michigan Transportation Research Institute
2901 Baxter Road
Ann Arbor, MI 48152
uumtri-ccat@umich.edu
(734) 763-2498
www.ccat.umtri.umich.edu

## TECHNICAL REPORT DOCUMENTATION PAGE

| 1. Report No. | 2. Government Accession No. | 3. Recipient's Catalog No. |
|---|---|---|
| ICT-21-039 | N/A | N/A |

| 4. Title and Subtitle | 5. Report Date |
|---|---|
| Passive Sensing of Electromagnetic Signature of Roadway Material for Lateral Positioning of Vehicle | November 2021 |
| | **6. Performing Organization Code** N/A |
| **7. Author(s)** Sachindra Dahal, Jeffery R. Roesler | **8. Performing Organization Report No.** ICT-21-039 UILU-ENG-2021-2039 |
| **9. Performing Organization Name and Address** Illinois Center for Transportation Department of Civil and Environmental Engineering University of Illinois at Urbana–Champaign 205 North Mathews Avenue, MC-250 Urbana, IL 61801 | **10. Work Unit No.** N/A |
| | **11. Contract or Grant No.** Grant No. 69A3551747105 |
| **12. Sponsoring Agency Name and Address** Center for Connected and Automated Transportation University of Michigan Transportation Research Institute 2901 Baxter Road Ann Arbor, MI 48152 | **13. Type of Report and Period Covered** Final Report |
| | **14. Sponsoring Agency Code** Center for Connected and Automated Transportation |

**15. Supplementary Notes**

Funding under Grant No. 69A3551747105 U.S. Department of Transportation, Office of the Assistant Secretary for Research and Technology (OST-R), University Transportation Centers Program.
https://doi.org/10.36501/0197-9191/21-039

**16. Abstract**

Autonomous vehicles (AV) and advanced driver-assistance systems (ADAS) offer multiple safety benefits for drivers and road agencies. However, maintaining the lateral position of an AV or a vehicle with ADAS within a lane is a challenge, especially in adverse weather conditions when lane markings are occluded. For significant penetration of AV without compromising safety, vehicle-to-infrastructure sensing capabilities are necessary, especially during severe weather conditions. This research proposes a method to create a continuous electromagnetic (EM) signature on the roadway, using materials compatible with existing paving materials and construction methods. Laboratory testing of the proposed concept was performed on notched concrete-slab specimens and concrete prisms containing EM materials. An induction-based eddy-current sensor and magnetometers were implemented to detect the EM signature. The detected signals were compared to evaluate the effects of sensor height above the concrete surface, type of EM materials, EM-material volume, material shape, and volume of EM concrete prisms. A layer of up to 2 in. (5.1 cm) of water, ice, snow, or sand was placed between the sensor and the concrete slab to represent adverse weather conditions. Results showed that factors such as sensor height, EM-material volume, EM dosage, types of the EM material, and shape of the EM material in the prism were significant attenuators of the EM signal and must be engineered properly. Presence of adverse surface conditions had a negligible effect, as compared to normal conditions, indicating robustness of the presented method. This study proposes a promising method to complement existing sensors' limitations in AVs and ADAS for effective lane-keeping during normal and adverse weather conditions with the help of vehicle-to-pavement interaction.

| 17. Key Words | 18. Distribution Statement |
|---|---|
| Autonomous vehicles, advanced driver-assistance systems, intelligent transportation system, vehicle-to-infrastructure communication, concrete | No restrictions. This document is available through the National Technical Information Service, Springfield, VA 22161. |

| 19. Security Classif. (of this report) | 20. Security Classif. (of this page) | 21. No. of Pages | 22. Price |
|---|---|---|---|
| Unclassified | Unclassified | 31 | N/A |

**Form DOT F 1700.7 (8-72)** **Reproduction of completed page authorized**

# ACKNOWLEDGMENT, DISCLAIMER, MANUFACTURERS' NAMES

This project was conducted in cooperation with the Center for Connected and Automated Transportation and the Illinois Center for Transportation. The contents of this report reflect the view of the authors, who are responsible for the facts and the accuracy of the data presented herein. The contents do not necessarily reflect the official views or policies of CCAT or ICT. This report does not constitute a standard, specification, or regulation. Trademark or manufacturers' names appear in this report only because they are considered essential to the object of this document and do not constitute an endorsement of the product by CCAT or ICT. The authors also acknowledge Jordan Ouellet for his help with 3D printing the brackets for the sensors.

# TABLE OF CONTENTS

# LIST OF FIGURES

# LIST OF TABLES

# CHAPTER 1: INTRODUCTION

Connected and autonomous vehicles (AV) are on the verge of significantly altering the means of transportation of passengers, goods, and services, as well as vehicle interaction. The roadway infrastructure can no longer be seen as just a corridor design for the driver's mobility but also an active part in assisting vehicle guidance, control, and navigation. Adoption of advanced driver-assist systems (ADAS) or AV technologies has reported benefits such as improving driver/passenger safety, greater roadway capacity, and reducing traffic congestion and vehicle-fuel consumption (Anderson et al., 2016; Burns & Shulgan, 2018; Folsom, 2012; Greenblatt & Shaheen, 2015; Taiebat et al., 2018). AVs employ a suite of sensors such as RADAR, LIDAR, GPS, cameras, and ultrasonic sensors to perceive the roadway/roadside environment in order to control, guide, and navigate the vehicle independently of the driver (Burns & Shulgan, 2018; Ilas, 2013). Although, millions of miles have been driven by AV using these advanced sensors (Anderson et al., 2016; Burns & Shulgan, 2018; Kalra & Paddock, 2016), one of the main challenges of large-scale implementation of AV is the robustness of these systems in adverse weather conditions. Most of the existing AV sensors have severe limitations during weather such as heavy rain, snow, fog, and ice.

Lane-keeping of a vehicle is challenging, especially in nonideal conditions. Currently, AVs use GPS coordinates and cameras to maintain the vehicle's position in the travelling lanes (Schreiber, et al., 2013; Tao et al., 2013a, 2013b). Sensor fusion of multiple sensors such as GPS, camera, LIDAR, and 3D maps is effective in ideal conditions (Schreiber, et al., 2013; Tao et al., 2013b). Unfavorable lighting, occlusion, and adverse weather conditions make lane-marking detection and lane-keeping difficult. For example, GPS signals worsen (Cui & Ge, 2003; Dana, 1997; Milanés et al., 2008; Rodríguez-Pérez et al., 2007), lane markings are not clearly visible, and sensors such as LIDAR and cameras underperform during severe weather. In addition, tunnels and urban canyons block the direct signal for GPS, leading to reduced or no signal (Eskandarian et al., 2020; Gu et al., 2016). Algorithms to detect lanes better and thereby improve vehicle lateral positioning during adverse weather and/or reduced illuminance have been researched extensively (Álvarez et al., 2008; Caltagirone et al., 2019; Helala et al., 2012; Hoang et al., 2016; Janai et al., 2020; Khan et al., 2020; Pan et al., 2018; Tao et al., 2013b). However, lateral-positioning accuracy of vehicles during adverse weather is still a primary hurdle for wide-scale implementation of AVs, primarily due to difficulty in perception of lane markings by optical sensors or impractical time required for software corrections. The decreased perception by multiple sensors worsens the lane-keeping ability in critical conditions like snow and rain and increases risk of an accident due to vehicle departure from the lane. A solution that enables the pavement and vehicle to interact and determine its lateral position in these conditions would provide reliable, robust, and safe vehicle operation. Limited research has been done on this topic to establish pavement and vehicle interaction in order to assist in AV lateral positioning (Moreno-Navarro et al., 2019).

Different solutions have been proposed, with varying degrees of success to handle missing lane boundaries, using the geometric features of the lane (Janai et al., 2020; Khan et al., 2020). However, mitigating the effect of fog, rain, or snow for vision-based sensors has achieved limited success (Aldibaja et al., 2017; Bahnsen & Moeslund, 2019; Janai et al., 2020; Jiang et al., 2019; Liu et al., 2018; Ren et al., 2019; Zhu et al., 2017). A potential solution to help with lane-keeping during adverse

weather is communication with roadside units or embedding sensors in the pavement (Horani & Rawashdeh, 2019). Embedding a large number of sensors will significantly increase the cost and duration of construction and requires long-term maintenance of sensors for high reliability. Moreover, the sensor position affects power demand and its reliability over time. Additionally, sensors can lead to pavement distresses. These reasons make such an option less favorable for infrastructure owners and operating agencies. Roadside units are another choice to maintain vehicle position but are a prohibitively expensive addition to require on 6 million miles of roads in the United States.

Pavements are currently designed and constructed without consideration of active or passive communications with AVs. Modification of future pavements to enable communication with the AV is necessary for safe and wide-scale deployment. Pavements can adopt active or passive methods to connect and communicate with AV. Active-communication methods involve embedding sensors such as transponders or radio-frequency identification (RFID) in the pavement or installing sensors in the roadside infrastructure to assist the vehicle guidance. Passive-communication methods can be defined as modification of the roadway, such as lane markings or pavement-material properties, to create a unique and repeatable signature that AV can identify accurately as a secondary control and guidance system.

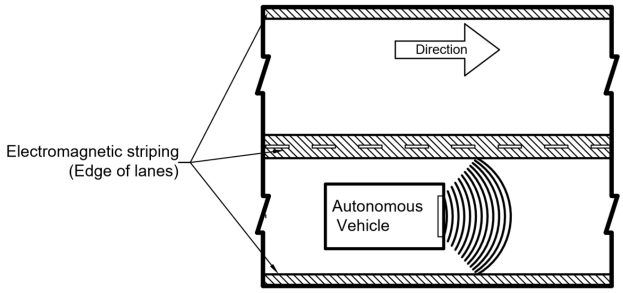


(a) Electromagnetic stripping on edge of lane

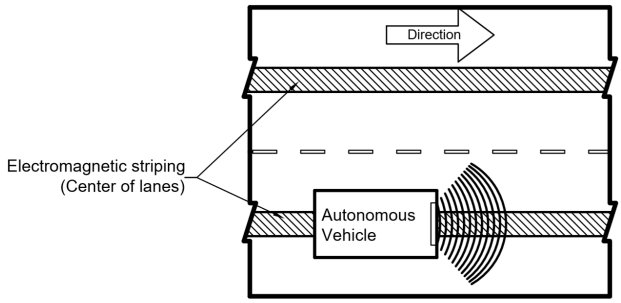


(b) Electromagnetic stripping on center of lane.

**Figure 1. Diagrams. Modifying pavement signature (markings or materials) to detect lateral roadway position of AV.**

The robustness of AV control and guidance depends on integration of redundant information from various sensors (Skog & Handel, 2009). To assist AV lateral positioning and, subsequently, control and

guidance, existing and new pavements can be modified to have passive-sensing capability by changing measurable material properties in the transverse profile, as presented in Figure 1. This study proposes a passive-sensing solution by modifying electromagnetic-material properties to create a continuous electromagnetic (EM) signature in the concrete or asphalt pavement to assist in AV lateral localization. Such EM signatures are created using materials that are commonly used in pavement construction and can be detected by an onboard vehicle sensor to control the lateral position of the vehicle within the lane. Due to no power requirement to maintain such EM signatures on the road, integrating into new pavement or during rehabilitation of pavement is comparatively easier than embedding active sensors, which require more planning, maintenance, and likely much higher costs. The study explores the effect of different EM materials, geometry of EM materials, dosage and volume of EM materials, and height of the vehicle sensors above the EM material on the signal strength. Laboratory specimens and tests are developed and performed to create and detect such an EM signature. In addition, robustness of the proposed EM signature and sensor combination is tested when water, ice, snow, or sand—which can potentially attenuate current AV perception capabilities—is present between the surface of the specimen and sensor.

## RESEARCH SIGNIFICANCE AND SCOPE

This research proposes an innovative passive-sensing approach to localize AV within the lane by creating an EM signature in the near-surface pavement material. To achieve this goal, the top few inches of paving materials are modified so that onboard vehicle sensors can identify EM-property changes in the transverse cross section of the pavement. Laboratory tests are required to identify the sensing system, as well as potential EM-material types. The EM-modified paving material and sensing system are then lab tested with normal and adverse surface conditions.

Specific research goals of this report are as follows:

- Identify EM materials that can modify existing EM properties of pavement surface (concrete and asphalt), specifically electrical conductivity and/or magnetic permeability.
- Identify an appropriately sensitive sensing system that can detect changes in transverse EM properties of concrete or asphalt in a laboratory specimen.
- Prepare laboratory specimens of different geometries and EM-material volume to create a detectable and repeatable EM signature.
- Detect EM signature in the laboratory specimen using the sensing systems in normal and adverse conditions.

# CHAPTER 2: PASSIVE EM-SENSING SYSTEMS: PRINCIPLES

Currently, cameras are the primary mode in AVs to detect lane marking and guide vehicles. These optical systems rely on visible features on the roadway to guide the vehicle properly. A road without lane markings or clear lane edges would present a much more difficult guidance and control problem for AVs. Furthermore, the presence of dirt, shadows, unfavorable lighting conditions, and adverse weather conditions on the pavement surface obstructs detection of optical features and necessitates a more robust method.

Contactless passive-sensing systems that can detect paving material property changes is required. Moreover, the system should be able to handle the limitations of current perception systems. Detection of thermal differences on the pavement surface using an infrared thermal-imaging camera is one example of a passive-detection approach, but surface-temperature variations would be hard to maintain over time without a significant change in the lateral thermal properties of the pavement-surface materials. Embedded passive RFID tags in the pavement would require significant modification of the existing pavement-surface layer, and the number of sensors required for accurate lateral and longitudinal positioning between sensors limits their practical implementation. EM properties of materials are generally not disturbed by physical obstructions such as lighting conditions, shadows, and dirt/debris; and such properties can be detected when submerged in water or covered in ice—with a proper sensing device. Induction-based eddy-current sensors and magnetometer sensors, which detect changes in the pavement's EM properties (electric conductivity and magnetic permeability) are discussed in this section as two alternatives to detect such EM-property variations.

As pavements are not currently designed to create distinct EM signatures, the pavement surface has nearly uniform electrical properties in both the transverse and longitudinal direction. Addition of conductive metallic fibers or larger metallic particles changes electric conductivity and magnetic permeability of the pavement. The higher electric conductivity can lead to induction of eddy current once an external alternating magnetic field is applied. These eddy currents can be detected by an induction-based sensor, which will be described in more detail later.

In addition to electric conductivity, depending on the metal type, magnetic permeability also changes when metals are present. When a pavement has no modification to the EM properties, as presented in Figure 2(a), it can be assumed that a pavement has a relatively uniform magnetic force over a small segment, mainly due to the earth's magnetic field. The addition of higher amounts of ferrous materials (such as steel fibers) in certain locations of the pavement increases the magnetic permeability, which allows more magnetic lines to pass through that section, as compared to the standard pavement section. Introduction of EM material, for instance in the center of the lane, channelizes the magnetic lines of force, as presented in Figure 2(b). More magnetic flux now passes through the highly magnetically permeable ferrous metal rather than the standard pavement materials. Magnetometer sensors can detect such variations in the magnetic field, e.g., in the transverse direction of the pavement in Figure 2(b).

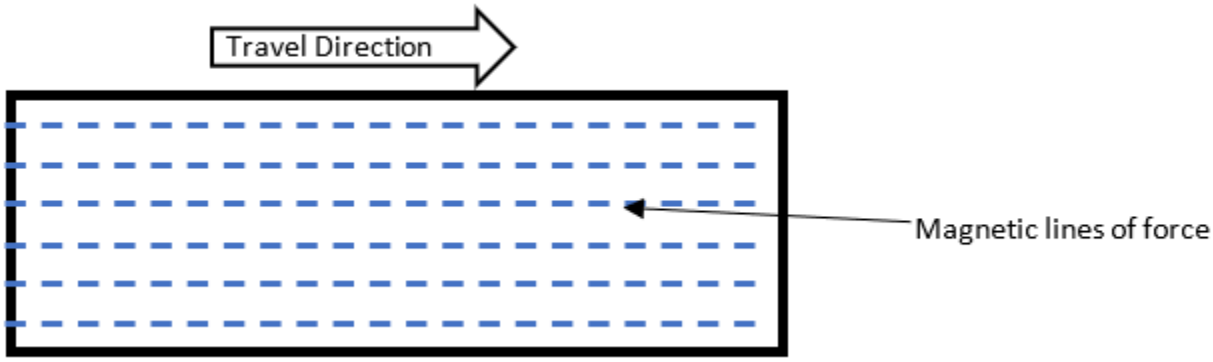


(a) Uniform magnetic lines of force

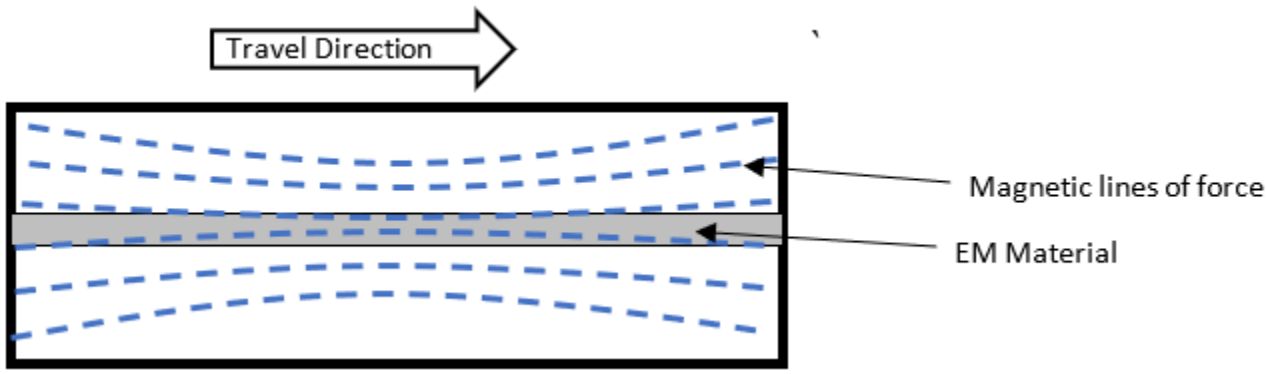


(b) Channelized magnetic lines due to EM material

**Figure 2. Diagrams. Uniform magnetic lines of force without EM signature in the pavement surface and channelized magnetic lines of force through the EM material of higher magnetic permeability in the center of the lane.**

## INDUCTION-BASED SENSORS

Eddy currents are induced within a conductor when it is subjected to changing magnetic fields. Devices such as metal detectors use pulse-induction techniques to create a varying magnetic field to identify the location of conducting metals. These techniques have been used to detect buried jewelry, historic artifacts, landmines, or unexploded ordinance (Kim et al., 2015).

An induction-based sensor consists of a transmitter coil with multiple loops of wire, forming an inductor. When electricity flows through the transmitter coil, a magnetic field is created around the coil. The sensor briefly energizes the coil, creating a static magnetic field by generating a pulse of DC voltage; then the voltage is rapidly cut off to collapse the magnetic field at a higher rate. These voltage pulses are generated and collapsed rapidly, as presented in Figure 3(a), by a negative input voltage (known as “flyback” voltage) about 205 times a second (i.e., 205 Hz). When the voltage rapidly collapses to flyback voltage, the rate of change of the magnetic field is highest and induces eddy currents in the metal target. The flyback voltage decays back exponentially to zero. When there is an eddy current induced in the nearby metallic target, the eddy current acts as a secondary

magnetic field that alters the flyback-voltage decay curve. For each pulse, the subtle voltage changes in the coil during this decay period because the eddy current in the metallic target is amplified and stored in a capacitor. The presence of the secondary magnetic field from the metallic target increases the charge stored in the capacitor, which otherwise decays to zero voltage in absence of a secondary magnetic field. The output of the circuit is a DC voltage with nominal value of about zero when no metallic target is present and a rise in the voltage in the presence of a secondary magnetic field (Kim et al., 2015; Medek et al., 2001; Overton & Moreland, 2012). A pulse-induction circuit, presented in Figure 3(b), with a coil size of 10 in. (25.4 cm) is used in this research to passively detect a section with higher conductance in a laboratory specimen.

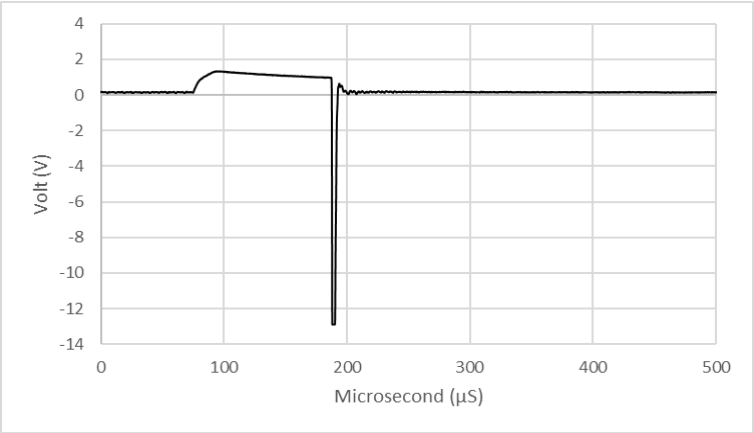


(a) Typical pulse generated by a pulse-induction circuit, showing short pulse and rapid collapse of signal to around –12 V.


(b)Pulse-induction circuit used in this research.

**Figure 3. Chart and photo. Typical pulse generated by a pulse-induction circuit and the circuit used in this research.**

## MAGNETOMETER

Magnetometers are devices that measure strength and direction of magnetic fields. This research employs fluxgate magnetometers, presented in Figure 4(c), which are highly sensitive sensors that measure magnetic field strengths of $10^{-10}$ to $10^{-4}$ Tesla (Ripka, 1992; You, 2018). The measurement range is sensitive enough to measure the disturbances in magnitude ($5 \times 10^{-7}$ Tesla) and direction of the earth's magnetic field.

Fluxgate magnetometers consist of a soft magnetic material core that has two sets of coils (drive and sense coil) wrapped around the core, as presented in Figure 4(a). Fluxgate action depends on the time variation of permeability of the core. The drive coil periodically drives the core to saturation in the positive direction, out of saturation, and to saturation in the negative direction due to the excitation current ($I_{exc}$). The process follows magnetic flux (B) versus magnetization force (H) hysteresis loop, presented in Figure 4(b). The magnetic permeability ($\mu$) of the core material changes significantly as the core is driven into and out of saturation. When the core is unsaturated, the ambient magnetic field ($B_0$) is channeled through the core due to the higher magnetic permeability in the core. When the excitation current is increased and the core reaches saturation, permeability of the core decreases; and the ambient magnetic flux is driven out of the core, leaving only the flux from the drive coil in the core. The saturation state where "gating" of the ambient flux occurs gives the name of the device, fluxgate magnetometer. During this process, the sense coil measures induced voltage ($V_{ind}$) caused by the inflow and outflow of the external flux as the core goes into and out of saturation. The induced voltage is proportional to the measured magnetic field (Evans, 2006; Moreland, 2002; Primdahl, 1979; Primdahl, 1970; Ripka, 1992).

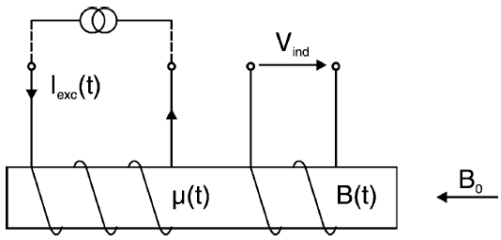


(a) Core with sense and drive coil

***Source: Ripka, 2003***

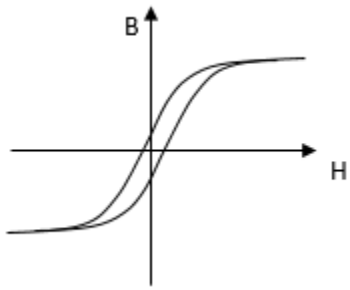


(b) B-H hysteresis curve for the core material

***Source: Inspired by Primdahl, 1970***


(c) Magnetometer used for this study

**Figure 4. Diagrams and Photo. Core with sense and drive coil (a), B-H hysteresis curve (b), and magnetometer sensor used for the study (c).**

## MATERIAL SELECTION

Suitable materials to modify electrical conductivity and/or magnetic permeability of pavement at the target location were identified. Increasing the paving material's electric conductivity should develop eddy current in these materials when an induction-based sensor is applied. All the ferrous materials increase magnetic permittivity of asphalt or concrete, allowing channelization of the earth's magnetic flux. Assuming uniform magnetic flux over the pavement, localized ferrous material fluctuates the magnetic field that a magnetometer can sense. Materials that are already used in pavement construction and can modify such EM properties would be ideal candidates for constructability and acceptance. Additionally, other alternative materials are also explored as candidates for creating an EM signature in pavement-surface layers.

The pavement-construction industry already uses steel fibers and, in some applications, steel-slag aggregates (Roesler et al., 2019), which contain ferromagnetic material. The presence of metal in these construction materials makes them a good material candidate to investigate. Likewise, adding iron powder (Fe) or iron-oxide ($Fe_3O_4$) powder into cement/asphalt (Arabani & Mirabdolazimi, 2011; Ghannam et al., 2016) prior to construction could also be an alternative. Metglas 2714A, referred to in this report as *metglas*, is a commercially available, very highly magnetic permeable material that is also tested in three shapes—ribbon, fiber, and powder—using the magnetometer. The metglas ribbon was adhered to the top surface of the lab specimens, while the fiber and powder forms of metglas were mixed with the concrete during the casting of the EM prism. The degree of change of EM properties depends on size/geometry of the EM material, dosage level of the EM material, and the volume of host material containing EM materials. This lab study tests EM materials incorporated at three dosages to analyze the effect on the EM signature detected by the two types of sensors.

EM materials, their shape and dimensions, along with sensors used to test the materials, are presented in Table 1. The localized presence of any of the proposed material in Table 1 can increase electric conductivity of the paving material. Due to the very high magnetic permeability of metglas, all of the shapes of metglas were tested only with the magnetometer, while other materials were tested using both sensors.

**Table 1. Material Description for EM Property Modifications.**

| Material | Form/Shape | Dimension | Sensors used |
|---|---|---|---|
| Steel Fiber | Cylindrical | Length: 50 mm<br>Diameter: 1.35 mm | Magnetometer, induction-based eddy |
| Iron Filing | Powder | Diameter: 420 µm | Magnetometer, induction-based eddy |
| Iron Oxide ($Fe_3O_4$) | Powder | Diameter: 37 µm | Magnetometer, induction-based eddy |
| Metglas | Ribbon | Width: 38 mm<br>Thickness: 1.5 µm | Magnetometer |
| Metglas | Prismatic | Width: 5 mm<br>Length: 38 mm<br>Thickness: 1.5 µm | Magnetometer |
| Metglas | Powder | Diameter: 850 µm | Magnetometer |

## LABORATORY-SPECIMEN PREPARATION

Three notched slabs of the dimensions 18-in. (45.7-cm) width, 18-in. (45.7-cm) length, and 6-in. (15.2-cm) depth were cast in the laboratory with normal concrete, as presented in Figure 5. Each slab's notch was filled with a removable concrete prism made with the one of the EM materials in Table 1. The notch dimensions and EM-modified material prism were of cross-sectional sizes 1 x 1 in. (2.54 x 2.54 cm), 2 x 2in. (5.1 x 5.1 cm), and 3 x 3 in. (7.6 x 7.6 cm) and will be referred in this report as 1 x 1, 2 x 2, and 3 x 3 prisms respectively. These prisms will evaluate the detection capabilities of different relative volumes of EM material in the host paving material.

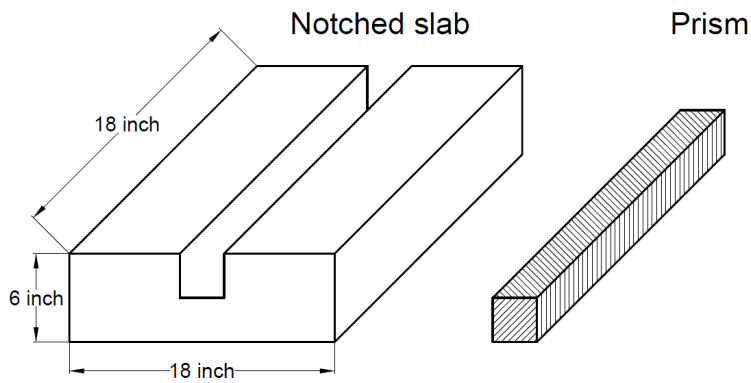


**Figure 5. Diagram. Notched concrete-slab specimen with EM-modified prism corresponding to the notch dimensions.**

## TEST SETUP AND VARIABLES

A motorized frame was constructed (see Figure 6) that moves the sensor laterally above the notched slab filled with EM prisms. Sensor reading from lateral motion over the sample shows how EM signature changes in the transverse direction can be utilized by a vehicle to determine lateral position in a lane.

The eddy-current sensor coil is mounted so the plane of the coil is parallel to the slab surface (Figure 6(a)) to maximize the induction of eddy current in the target location. For magnetometers, a sensor-array platform was made, with magnetometers arranged in gradiometer style. Vertical gradiometers have two or more magnetometers separated vertically by a certain distance such that the sensor on top measures the overall magnetic noise due to the environment and the sensor on bottom measures the magnetic signal due to both the EM material and environmental magnetic noise. For this research, the magnetometers are mounted in parallel vertically and separated axially by 10 in, (25.4 cm) (Figure 6(b)) to form a gradiometer. When the reading of the top sensor is subtracted from that of the bottom sensor, the magnetic noise due to the environment is canceled, producing the effect of the EM material in disturbing the magnetic field (Clark, 1990; Ernenwein & Hargrave, 2009). Data are collected at the rate of 500 Hz for eddy-current sensor and at 2 kHz for the magnetometer, which is suitable for applications in AVs.

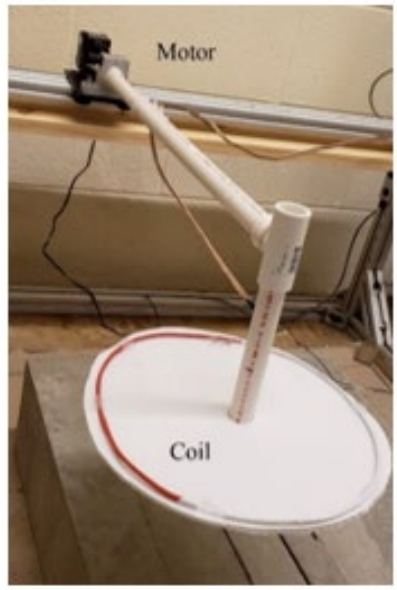


(a) Motorized induction-based eddy-current coil over the slab specimen

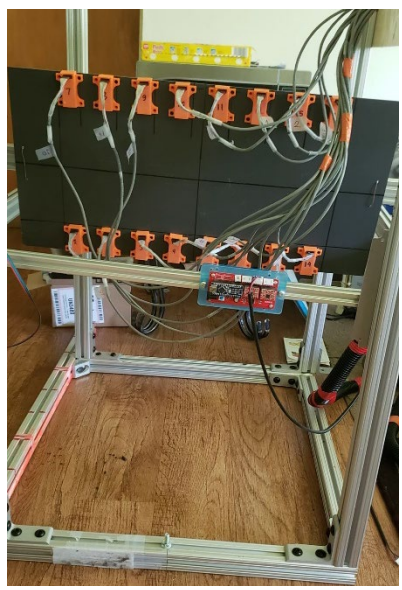

(b) Magnetometer-sensor platform arranged in gradiometer formation

**Figure 6. Photos. Motorized induction-based eddy-current sensor and magnetometer-sensor platform.**

Table 2 provides the testing factorial conducted for the two sensor types, which were all the potential causes that reduce the signal strength. These factors are also significant contributors to achieving an optimal signal for implementation beyond the lab. To evaluate the role of each factor, the results from different variation levels are normalized to the maximum expected signal for each factor and compared.

**Table 2. Testing Factors Evaluated Using Two Types of Noncontact Sensors**

| Factors | Eddy-Current Sensor | Magnetometer | Remarks |
|---|---|---|---|
| Materials | Steel Fiber, Iron Powder, $Fe_3O_4$ | Steel Fiber, Iron Powder, $Fe_3O_4$, Metglas | Type of material and shape of material |
| Surface Condition | Ice, Water | Ice, Water, Sand, Snow | Each condition is tested at 0 in., 1 in., and 2 in. |
| Height of Sensor | 5 in., 6 in., 7 in. | 6 in., 9 in., 12 in. | Distance between the bottom of sensor and top of the slab |
| Notch Dimension | 1.5 in., 2.5 in., 3.5 in. | 1 in., 2 in., 3 in. | Cross section of notch and prism referred to as 1 x 1, 2 x 2, and 3 x 3, respectively. |
| Shape Variation | Not tested | Fiber/Cylindrical, Powder, Ribbon | Only metglas was tested using a fluxgate magnetometer. |
| Dosage of EM Material | 0.5%, 0.75%, 1% | 0.5%, 1%, 2% | EM-material percentage by volume of prism |

Note 1 inch = 2.54 cm

Each factor mentioned in Table 2 has varying degrees of effect on the expected signal strength. For instance, for both sensor types, a higher signal is expected when the distance between the sensor and the EM material is small; and conversely, the signal strength decreases as the distance increases. Table 3 presents the factors, along with different expected signal strength of high (variation 1), medium (variation 2), and low (variation 3) based on the variation of that factor level when all the other factors are kept constant. The results section presents the degree of impact of each factor when the obtained signals are normalized to the higher signal of that factor while other parameters are kept the same.

**Table 3. Expected Signal Strength (High, Medium, Low), Based on Various Factors Tested**

| Factor | Sensors | Variation 1 (Expected high signal) | Variation 2 (Expected medium signal) | Variation 3 (Expected low signal) |
|---|---|---|---|---|
| Material Type | Eddy, Fluxgate | Steel Fiber | Iron Powder | $Fe_3O_4$ |
| Height of Sensor | Eddy | 5 in. | 6 in. | 7 in. |
| Height of Sensor | Fluxgate | 6 in. | 9 in. | 12 in. |
| Notch Dimension | Eddy, Fluxgate | 3 x 3 | 2 x 2 | 1 x 1 |
| Dosage of EM material | Eddy | 1% | 0.75% | 0.50% |
| Dosage of EM material | Fluxgate | 2% | 1% | 0.50% |
| Shape variation (metglas only) | Fluxgate | Ribbon | Fiber | Powder |
| Surface Condition—Ice, Water | Eddy, Fluxgate | 0 in. | 1 in. | 2 in. |
| Surface Condition—Snow, Sand | Fluxgate | 0 in. | 1 in. | 2 in. |

Note: 1 inch = 2.54 cm

The effectiveness of EM-signal detection under adverse condition was tested by imposing a layer of adverse conditions on top of the notched slab with the EM prism. A plastic container was used to

hold water, snow, ice, and sand on top of the slab at two different thicknesses, 1 in. (2.54 cm) and 2 in. (5.1 cm). The test setup of the magnetometer with adverse conditions is presented in Figure 7. The plastic container was tested separately by both types of sensors to verify that it does not have any effect on the signal.

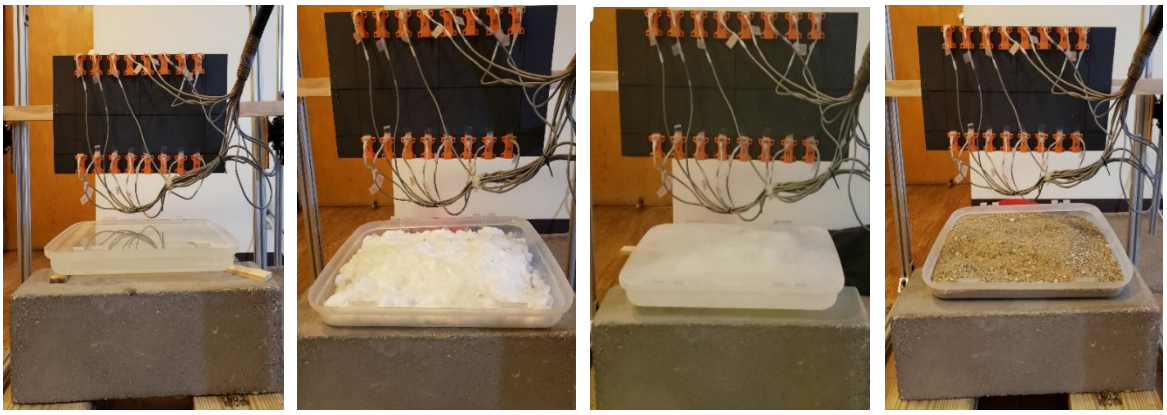

(a) Water (b) Snow (c) Ice (d) Sand

**Figure 7. Photos. Adverse condition of water, snow, ice, or sand imposed on top of the slab.**

# CHAPTER 3: RESULTS AND DISCUSSION

This chapter discusses the results from the two different sensors. For both sensor configurations, the motorized frame moves the sensor from one end of the notched slab to the other multiple times. The signal increases as it approaches the EM prism in the middle. The signal peaks above the prism and then starts to decrease as the sensor moves away from the EM prism to the other end of the frame. The sensor continues scanning the prism in the reverse direction and comes to the origin. The prisms are scanned multiple times in this sequence, which creates a continuous signal, as presented in Figure 8. The peak value of the signal is determined for each time the sensor is directly above the prism. These peak values are then averaged to measure a representative signal peak value to compare various factors.

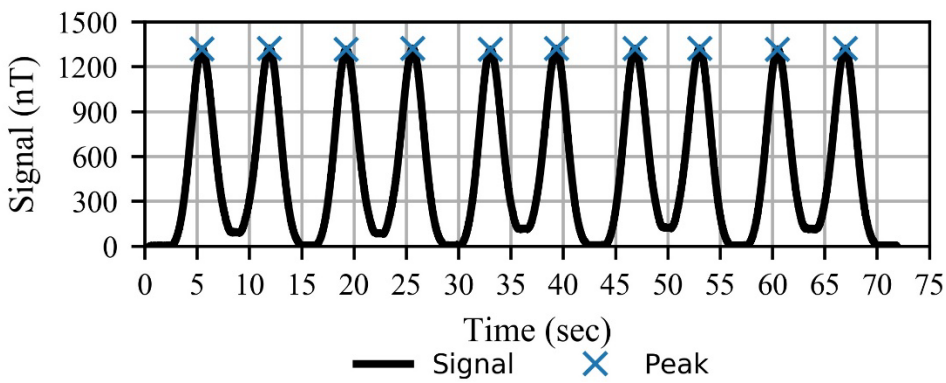


**Figure 8. Graph. Representative signal using magnetometer with detected peaks. Average of all the peak values is considered a representative signal value for one factor.**

## INDUCTION-BASED EDDY-CURRENT RESULTS

Figure 9 presents representative signals (nonnormalized) obtained from one scan over the slab at the three sensitivity levels for each factor. As expected, the signal strength depends on the lateral position of the sensor coil. The signal is highest when the coil center is above the EM prism and goes close to zero as the coil center is offset 10 to 15 cm from the center of the notch material. In general, the signal peak decreases as the sensitivity-variation level (presented in Table 3) goes from high (variation 1) to low (variation 3) expected signal for a given factor. Table 4 presents the three variations for each factor, along with the average peak signal in millivolt (mV) recorded by the induction-based eddy-current circuit. The EM prism of size 3 x 3, with a 1% dose of steel fiber measured from 5-in. (12.7-cm) height in the normal condition is considered as a standard. For each factorial testing, only that factor being test was varied, keeping other factors as standard. In addition, two variations with lower expected signals are normalized with respect to variation with higher expected signals (variation 1). The normalized values for each signal at different variation levels (high, medium, and low) are presented for each factor in Figure 10.

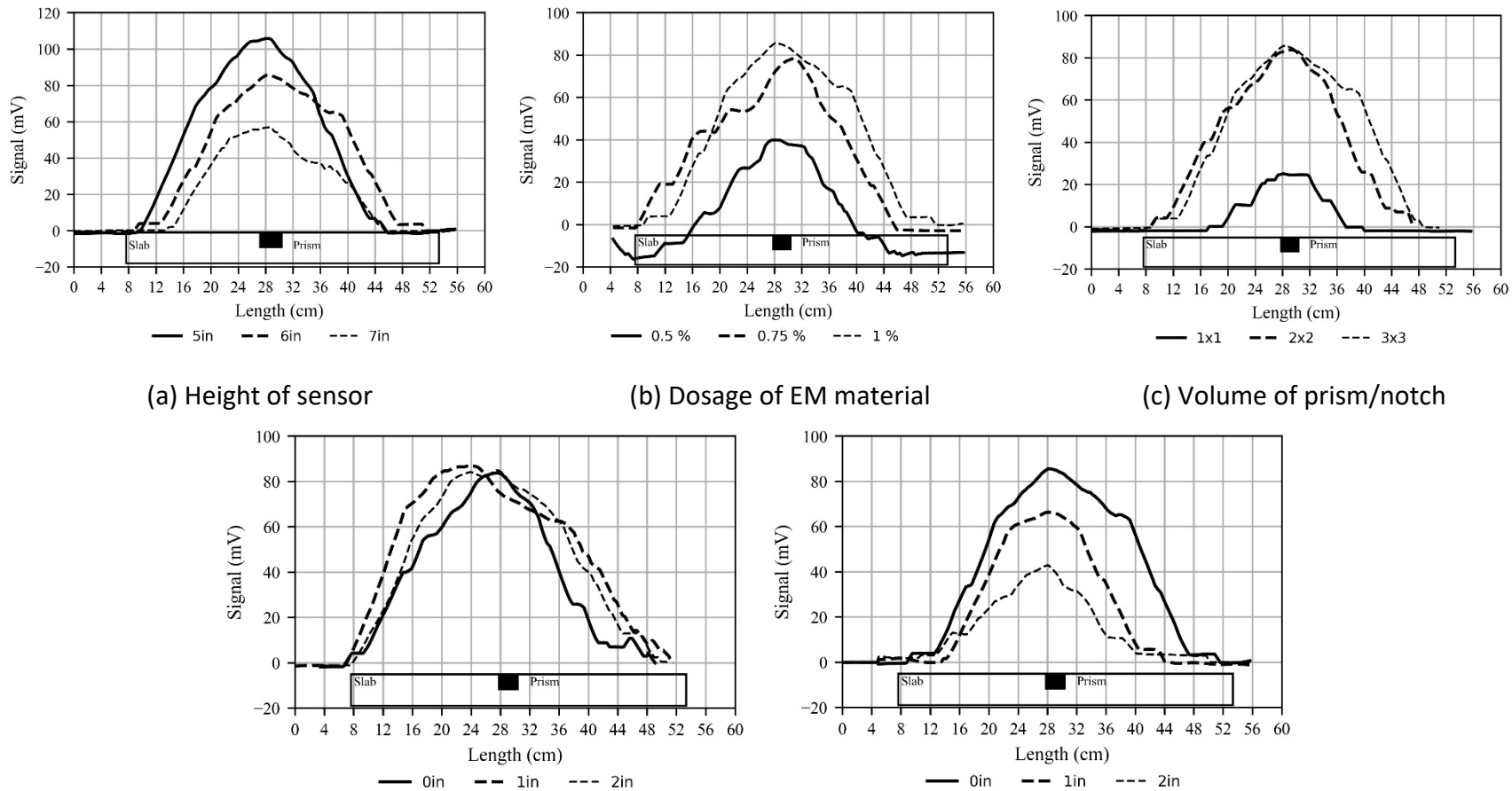


(a) Height of sensor (b) Dosage of EM material (c) Volume of prism/notch

(d) Standing ice on slab surface (e) Standing water on slab surface

**Figure 9. Graphs. Representative signals obtained from an induction-based eddy-current sensor, indicating one scan over the slab with EM signature for three sensitivity levels of each factor.**

**Table 4. Three Variations of Each Factor, Along with Signal (mV) Obtained by Eddy-Current Sensor and Normalized Values with Respect to Variation 1 for EM material (Steel Fibers)**

| Factor | Variation 1 | Signal (mV) Variation 1 | Normalized (%) Variation 1 | Variation 2 | Signal (mV) Variation 2 | Normalized (%) Variation 2 | Variation 3 | Signal (mV) Variation 3 | Normalized (%) Variation 3 |
|---|---|---|---|---|---|---|---|---|---|
| Material Type | Steel Fiber | 88 | 100 | Iron Powder | NA* | NA* | $Fe_3O_4$ | NA* | NA* |
| Height of Sensor | 5 in. | 92 | 100 | 6 in. | 67 | 73 | 7 in. | 42 | 46 |
| Notch Volume | 3 x 3 | 88 | 100 | 2 x 2 | 74 | 84 | 1 x 1 | 33 | 38 |
| Dosage of EM Material | 1% | 87 | 100 | 0.75% | 77 | 88 | 0.50% | 46 | 53 |
| Surface Condition: Ice | 0 in. | 84 | 100 | 1 in. | 80 | 96 | 2 in. | 79 | 95 |
| Surface Condition: Water | 0 in. | 88 | 100 | 1 in. | 84 | 95 | 2 in. | 75 | 85 |

* Not available: No signal was observed for iron powder and $Fe_3O_4$ powder.

Note: 1 inch = 2.54 cm.

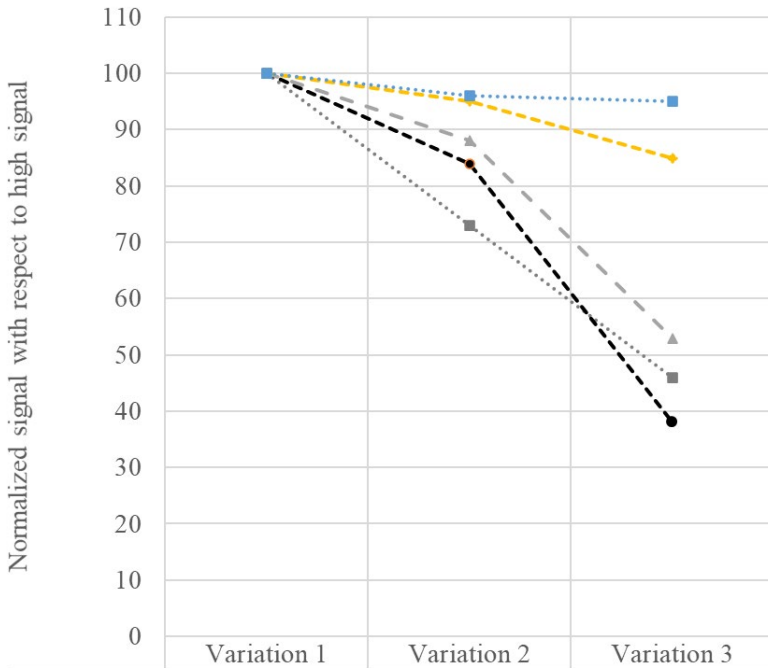


| | Variation 1 | Variation 2 | Variation 3 |
|---|---|---|---|
| Height | 100 | 73 | 46 |
| Volume | 100 | 84 | 38 |
| Dosage | 100 | 88 | 53 |
| Water | 100 | 95 | 85 |
| Ice | 100 | 96 | 95 |

**Figure 10. Graph with key in table form. Comparison of three variation levels of each factor, normalized to the highest expected signal obtained using an induction-based eddy-current sensor for EM material (steel fibers).**

## MAGNETOMETER RESULTS

Figure 11 presents a representative nonnormalized signal from one scan over the slab at the three sensitivity levels for each factor, using the magnetometer. Height of sensor, volume of notch, and dosage of EM material are compared on EM prisms with steel fiber. Similar to the induction-based sensor findings, the signal is highest when the sensor is directly above the EM prism and goes close to zero as the sensor is offset from the center of the EM prism. In general, the signal peak decreases as the sensitivity-variation level goes from high (variation 1) to low (variation 3) expected signal for a given factor.

Among other things, the dosage of the EM material for the three material shapes are different. Only metglas was available in all the shapes. A ribbon-shaped metglas was cut into fiber shape and ground into powder shape (about 850 µm). The reason for the difference in dosage percentage for the different shapes was mainly due to workability problems encountered for the fiber-shaped metglas (see Figure 12). With 1% by volume of metglas fiber, the concrete mixture was extremely unworkable, resulting in an improper sample. The volume fraction of fiber was reduced to mix the fiber properly.

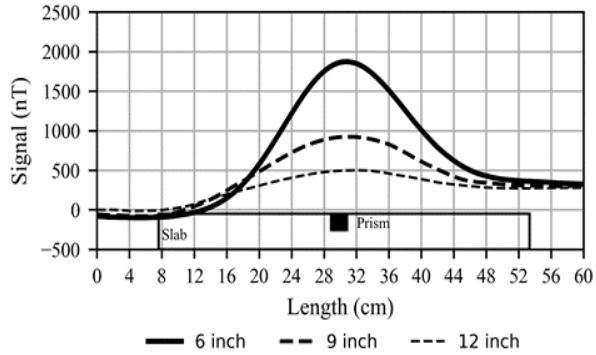


(a) Height of sensor

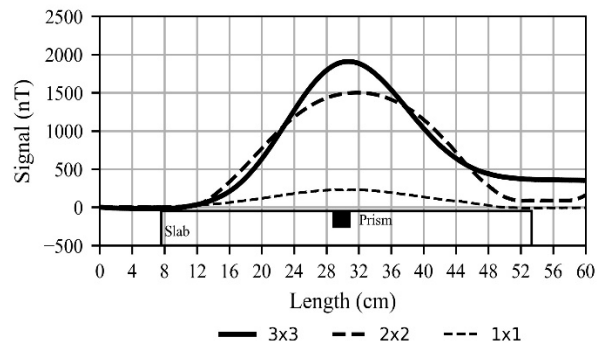


(b) Volume of notch/prism

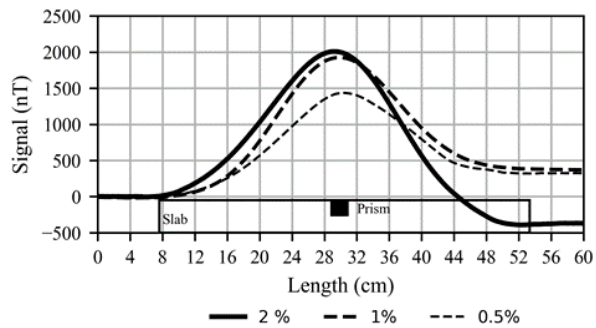


(c) Dosage of EM material

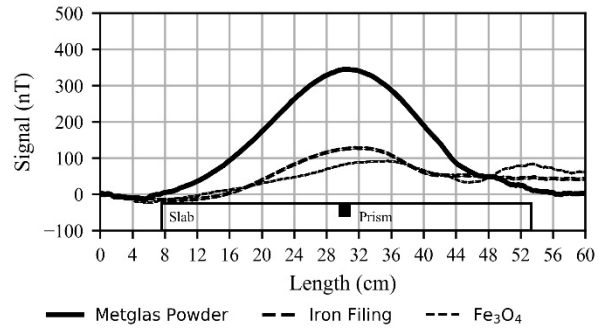


(d) Type of materials

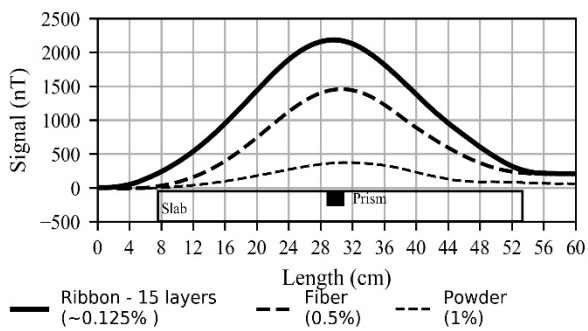


(e) Metglas material shape

**Figure 11. Graphs. Representative signals obtained from magnetometers, indicating one scan over the slab with EM signature for three sensitivity levels of each factor. Only steel fiber was used for (a), (b), and (c).**

**Figure 12. Photo. Unworkable concrete mixture with higher dosage of metglas fiber.**

Figure 13 shows the signals with 2-in. (5.1-cm) thickness of different adverse conditions imposed on top of the slab relative to the standard conditions. The EM prism of size 3 x 3 with 1% steel-fiber dose was tested from the height of 6 in. (15.2 cm) for all conditions. All the signals are very comparable in shape and magnitude, which demonstrates that the proposed EM method works even during adverse conditions encountered on pavements.

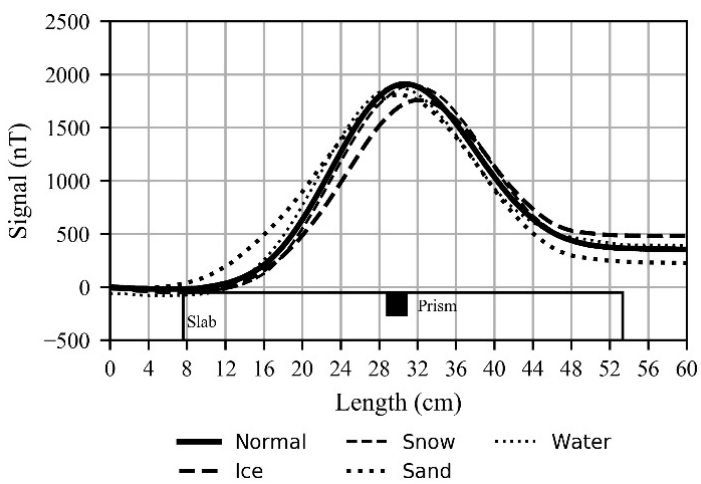


**Figure 13. Graph. Representative signals when the adverse condition of 2 in. (5.1 cm) of snow, water, ice, or sand is imposed on top of the slab with the EM prism, along with the normal condition.**

Figure 14 presents representative signals obtained when the notched concrete slab without the EM prism is tested, as well as signals obtained when asphalt of similar dimensions of notched slab is tested. Moreover, when nothing (or just air) is placed under the sensor, the signal is similar. No

noticeable differences are observed in the signal for these cases, which suggests that any EM signals observed are solely due to EM materials and not due to the host materials such as asphalt or concrete. In addition, it can be concluded that irrespective of host materials—asphalt or concrete—EM materials will have similar signals.

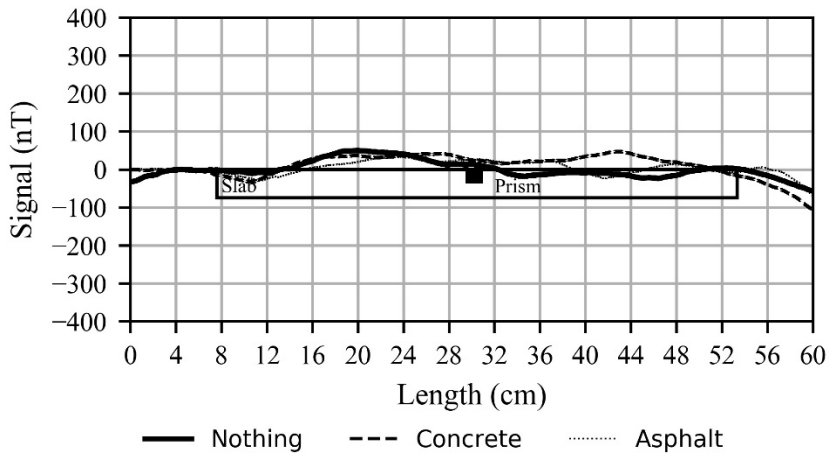


**Figure 14. Graph. Signals acquired for standard concrete and asphalt without EM material, and for no material (air).**

Table 5 presents the three variations for each factor, along with the average peak signal in nanotesla (nT). The standard cases in Table 5 are with 3 x 3 EM prisms with 1% steel fibers scanned from the height of 6 in. (15.2 cm). For each factorial testing, only that factor being tested was varied, keeping other factors as standard. The two variations with lower expected signals are normalized with respect to the variation with the higher expected signal (variation 1) for each factor. The normalized values for each signal-sensitivity level (high, medium, and low) are presented for each factor in Figure 15.

**Table 5. Three Variations of Each Factor, Along with Signal (nT) Obtained by Magnetometer and Normalized Values with Respect to Variation 1 for Steel Fibers, Unless Noted**

| Factor | Variation 1 | Signal (nT) Variation 1 | Normalized (%) Variation 1 | Variation 2 | Signal (nT) Variation 2 | Normalized (%) Variation 2 | Variation 3 | Signal (nT) Variation 3 | Normalized (%) Variation 3 |
|---|---|---|---|---|---|---|---|---|---|
| Height of Sensor | 6 in. | 1,815 | 100 | 9 in. | 924 | 51 | 12 in. | 447 | 25 |
| Notch Dimension | 3 x 3 | 1,815 | 100 | 2 x 2 | 1480 | 82 | 1 x 1 | 261 | 14 |
| Dosage of EM Material | 2% | 2031 | 100 | 1% | 1815 | 89 | 0.50% | 1,193 | 59 |
| Material Type | Metglas Powder | 345 | 100 | Iron Powder | 171 | 49 | $Fe_3O_4$ | 147 | 43 |
| Shape Variation | Ribbon | 2,172 | 100 | Fiber | 1,642 | 76 | Powder | 345 | 16 |
| Surface Condition: Ice | 0 in. | 1,815 | 100 | 1 in. | 1,714 | 94 | 2 in. | 1,742 | 104 |
| Surface Condition: Snow | 0 in. | 1,815 | 100 | 1 in. | 1,764 | 97 | 2 in. | 1,884 | 96 |
| Surface Condition: Water | 0 in. | 1,815 | 100 | 1 in. | 1,777 | 98 | 2 in. | 1,830 | 101 |
| Surface Condition: Sand | 0 in. | 1,815 | 100 | 1 in. | 1,758 | 97 | 2 in. | 1,768 | 97 |

Note: 1 inch = 2.54 cm.

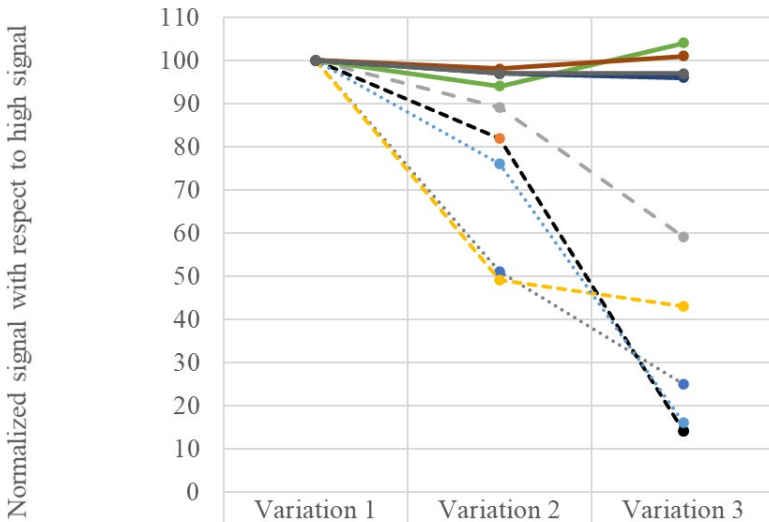


| | Variation 1 | Variation 2 | Variation 3 |
|---|---|---|---|
| Height | 100 | 51 | 25 |
| Volume | 100 | 82 | 14 |
| Dosage | 100 | 89 | 59 |
| Material type | 100 | 49 | 43 |
| Shape | 100 | 76 | 16 |
| Ice | 100 | 94 | 104 |
| Snow | 100 | 97 | 96 |
| Water | 100 | 98 | 101 |
| Sand | 100 | 97 | 97 |

**Figure 15. Graph with key in table form. Comparison of three variation levels of each factor, normalized to highest expected signal obtained using a magnetometer.**

## OBSERVATIONS AND DISCUSSION OF TEST RESULTS

Comparison of signals from the two types of sensors showed that different factors have different sensitivity in affecting the signal. This section compares the role and trend of all the factors presented above, as well as presents features and limitations of both sensors.

### Sensor Height

The signal strength has an inverse relation with the height of the sensor above the slab. The greater sensor height from the EM material leads to a weaker signal, as observed for both sensor types. Moreover, the magnetometer could sense the EM material from a much higher height, 12 in. (30.5 cm), than the eddy-current sensor, 7 in. (17.8 cm).

### Volume of Notch/Prism

For both sensors, the larger volume of notch/prism produced a better signal. Reduction of prism size from 3 x 3 to 2 x 2 reduced the signal strength by about 20% for both sensor types. However, a more significant drop was seen for both sensors with further reduction of prism size to 1 x 1, which dropped the signal to 38% and 14% of that obtained for the 3 x 3 prism, respectively, for the eddy-

current sensor and the magnetometer. For both of the sensor types, this drop of signal was the most significant among all the factors compared in this study.

## EM-Material Dosage

Higher EM-material dosage provided better signal for both sensor types. Among other factors, excluding adverse conditions, the signal was less sensitive to the dosage in both sensor types. This implies that with the right combination of other factors, even lower dosages of EM material can provide good signal.

## Material Type

The role of several material types was tested only with magnetometers. All three material types tested—metglas, iron filing, and iron oxide ($Fe_3O_4$)—were in powder form. Metglas, which had the highest magnetic permeability among the three materials, provided good signal strength, followed by iron filing and iron oxide ($Fe_3O_4$). The results imply that selection of the proper material type that is more responsive to the sensor is crucial, as the signal can decrease by more than 50% when using a less ideal material type. Appropriate material selection could also potentially lead to a lower prism volume or a reduced dose of EM material.

## Material Shape/Size

Three material shapes of metglas were tested using the magnetometer. The ribbon-shaped, flat-surface-type material had the highest signal when adhered to the prism surface, followed by metglas fiber and metglas powder, which were mixed with the fresh concrete. Despite larger EM-material dosages for the fiber shape and powder form (0.5% and 1%, respectively, as compared to the lower dosage of 0.125% of the ribbon shape), the signal was much weaker. The change in signal strength demonstrates the importance of selecting appropriate shape and size of the EM material. Material shape produced the most significant differences in EM signal, among all factors with exception of the volume of material.

Induction-based eddy current could not detect the presence of the powder form of iron and iron oxide ($Fe_3O_4$). The main reason for this failure to detect was the fine powder was uniformly distributed within the concrete material, making noncontinuous smaller segments of the conductive metal that was not large enough to generate detectable eddy current. Moreover, the iron powder and iron oxide ($Fe_3O_4$) are not ideal choices for an electric conductor, as compared to copper or steel fibers.

## Adverse Conditions

The presence of up to 2 in. (5.1 cm) of water and ice did not attenuate the signal significantly for either sensor type. For the eddy current, 2 in. (5.1 cm) of water reduced the signal by about 15%, as compared to the ideal normal conditions. However, for the magnetometer, the presence of ice, snow, water, or sand up to 2 in. (5.1 cm) changed the peak signal magnitude by less than 5%, as compared to normal conditions. Given the ability to detect such EM signature even with the imposed adverse conditions, the proposed method is promising for testing in larger-scale settings with vehicles as a secondary lane-keeping assist system for AVs.

## Host Materials

Both normal concrete and asphalt do not produce measurable signals by themselves with either sensor, and thus the addition of EM materials is linked to the improved signal strength. Signals for both asphalt and concrete are similar to that when nothing (or air) is placed under the sensor while scanning within the testing frame. As both pavement construction materials are similar to air with respect to the dielectric properties and magnetic permeability, both can be used as a host material to bind EM materials to create the detectable EM signature.

## Comparison of Sensors

Both sensors detect entirely different properties and have respective advantages and limitations. For practical purposes, a sensor that can operate effectively from the height of the bumper of a vehicle with minimum signal interference is ideal. Given the sensitivity of the induction-based eddy-current method with respect to the height of the sensor from the surface of the pavement, it could be a significant limitation in implementation. Moreover, the eddy-current method detects any type of metal that can conduct electricity. Thus, it can significantly be disturbed by bumpers and other parts of the car body made from aluminum and other metals. In contrast, magnetometers can detect only ferromagnetic metals such as iron, steel, cobalt, etc.; but they are sensitive to EM materials present even from larger distances away from the sensor. Table 6 summarizes the features and disadvantage of the two sensor types.

**Table 6. Features and Disadvantages of the Sensors**

| Sensors | Features | Disadvantage |
|---|---|---|
| Eddy-Current Sensor | • Active-sensing system: The sensor coil creates a varying magnetic field to detect the reflected signal.<br>• Depends on electric conductivity of the metal; therefore any metal that can conduct electricity can be detected. | • Vehicles have different metals near the location of the mounted sensor in the vehicle that can interfere with the signal.<br>• Lower sensor height for detection, as compared to magnetometer, limiting the application possibility.<br>• Standing water, which has high dielectric constant, can attenuate signal more. For instance, 2 in. of standing water reduced the signal by 15%. |
| Magnetometer | • Passive-sensing system: Nothing is projected to the environment.<br>• Depends on the magnetic permeability of material.<br>• Signal is not sensitive to non-ferromagnetic metal such as aluminum or copper that can be present in bulk in a vehicle body.<br>• Higher sensor height for detection. | • Environmental noise can affect the signal. Such noise can be removed by signal processing or a sensor-in-gradiometer arrangement and signal processing.<br>• Senses vertically below the mounted location. Not a forward-looking sensor like camera. |

# CHAPTER 4: CONCLUSION

Connected autonomous vehicles (AVs) that include advanced driver-assist systems (ADAS) are evolving rapidly and will eventually penetrate into normal transportation operations. Lane-keeping by AVs has been a problem in unfavorable lighting, occlusion, and adverse weather conditions like rain, snow, and fog, due to improper or absence of perception of lane markings. Such intermittent gaps in the function of perception sensors make AVs unable to perform at a prescribed reliability or accuracy level and currently remain a challenge for large-scale implementation. Optical sensors and GPS have reduced reliability during adverse weather, necessitating a robust solution that works in all weather conditions. A passive roadway-sensing concept was proposed by creating a continuous electromagnetic (EM) signature on the road using materials that are compatible with current paving materials, as well as construction methods, so that it can be easily integrated during construction or rehabilitation of the pavement.

Laboratory testing was completed on notched-slab specimens that were infilled with concrete prisms containing electromagnetic (EM) materials. EM signature was created in the prisms using one of four materials: steel fibers, metglas, iron filing, or iron oxide ($Fe_3O_4$). Two sensing systems were used: (a) an induction-based eddy-current sensor and (b) magnetometers. The factors expected to impact the signal strength—such as the height of sensors above the surface, dosage of EM material, volume of EM prism, EM-material type, EM-material shape, and adverse conditions (ice, sand, water, and snow)—were tested systematically. Concrete, as well as asphalt materials, demonstrated comparable EM signature, which was much lower in magnitude than that of EM materials, meaning both concrete and asphalt can work as host materials.

The results from both sensors indicated that multiple material and geometric factors can be engineered to optimize the signal strength, such as height of sensor, dosage of EM material, volume of EM material, and geometry and types of EM materials. Improper selection of one or more of these factors would greatly reduce the signal strength. However, presence of adverse surface conditions with optimal sensor arrangement and EM material properties had negligible effect on the acquired signal. Approximately 2 in. (5.1 cm) of standing water attenuated up to 15% of signal in the eddy-current sensor. All four types of adverse conditions (sand, water, snow, and ice) affected the magnitude of signal by less than 5%, as compared to the normal condition in the case of the magnetometer. Features and limitations of both sensors were presented. Eddy-current sensors' main limitations were limited height above the EM-signature material for detection and its detection of any type of conductive metal near the sensor, which is problematic for most vehicle applications. Magnetometers were also affected by background environmental noise, but this can be alleviated by using the sensors in a gradiometer configuration.

The proposed approach of modifying a small, longitudinal slice of pavement to modify EM property is a promising means to detect the lateral position of AV, especially in adverse weather conditions. With proper material selection, considering all the factors that affect the signal, a continuous reliable and robust EM signature can be engineered by modifying a few inches of the top layer of the pavement surface. Such an EM signature enables passive pavement-and-vehicle communication and has the potential to increase the reliability of AV lane-keeping in all weather and road-surface conditions. If

successful in large-scale testing, the proposed method opens a new paradigm in pavement design where roadways in the future will not only be designed for physical properties but also for the EM properties on the surface.

# REFERENCES


Aldibaja, M., Suganuma, N., & Yoneda, K. (2017). Improving localization accuracy for autonomous driving in snow-rain environments. *SII 2016—2016 IEEE/SICE International Symposium on System Integration*, 212–217. https://doi.org/10.1109/SII.2016.7844000

Álvarez, J. M., López, A., & Baldrich, R. (2008). Illuminant-invariant model-based road segmentation. *IEEE Intelligent Vehicles Symposium, Proceedings*, 1175–1180. https://doi.org/10.1109/IVS.2008.4621283

Anderson, J., Kalra, N., Stanley, K., Sorensen, P., Samaras, C., & Oluwatola, O. (2016). Autonomous Vehicle Technology: A Guide for Policymakers. In *Autonomous Vehicle Technology: A Guide for Policymakers*. Rand Corporation. https://doi.org/10.7249/rr443-2

Arabani, M., & Mirabdolazimi, S. M. (2011). Experimental investigation of the fatigue behaviour of asphalt concrete mixtures containing waste iron powder. *Materials Science and Engineering A*. https://doi.org/10.1016/j.msea.2011.01.099

Bahnsen, C. H., & Moeslund, T. B. (2019). Rain removal in traffic surveillance: Does it matter? *IEEE Transactions on Intelligent Transportation Systems*, *20*(8), 2802–2819. https://doi.org/10.1109/TITS.2018.2872502

Burns, L., & Shulgan, C. (2018). *Autonomy: The Quest to Build the Driverless Car—And How It Will Reshape Our World*. HarperCollins.

Caltagirone, L., Bellone, M., Svensson, L., & Wahde, M. (2019). LIDAR–camera fusion for road detection using fully convolutional neural networks. *Robotics and Autonomous Systems*, *111*, 125–131. https://doi.org/10.1016/J.ROBOT.2018.11.002

Clark, A. (1990). Seeing Beneath the Soil. In *Seeing Beneath the Soil*. Taylor & Francis. https://doi.org/10.4324/9780203279304

Cui, Y., & Ge, S. S. (2003). Autonomous vehicle positioning with GPS in urban canyon environments. *IEEE Transactions on Robotics and Automation*, *19*(1), 15–25. https://doi.org/10.1109/TRA.2002.807557

Dana, P. H. (1997). Global Positioning System (GPS) Time Dissemination for Real-Time Applications. *Real-Time Systems*, *12*(1), 9–40. https://doi.org/10.1023/A:1007906014916

Ernenwein, E. G., & Hargrave, M. L. (2009). Archaeological Geophysics for DoD Field Use. In *Environmental Security Technology Certification Program (ESTCP)*. https://hdl.handle.net/11681/19355

Eskandarian, A., Wu, C., & Sun, C. (2020). Research Advances and Challenges of Autonomous and Connected Ground Vehicles. *IEEE Transactions on Intelligent Transportation Systems*, *22*(2), 683–711. https://doi.org/10.1109/TITS.2019.2958352

Evans, K. (2006). Fluxgate Magnetometer Explained—Mar. 2006. *Invasens (Internal)*. http://www.invasens.co.uk/FluxgateExplained.PDF

Folsom, T. (2012). Energy and Autonomous Urban Land Vehicles. *IEEE Technology and Society*

*Magazine*, *31*(2), 28–38. https://doi.org/10.1109/MTS.2012.2196339

Ghannam, S., Najm, H., & Vasconez, R. (2016). Experimental study of concrete made with granite and iron powders as partial replacement of sand. *Sustainable Materials and Technologies*. https://doi.org/10.1016/j.susmat.2016.06.001

Greenblatt, J. B., & Shaheen, S. (2015). Automated Vehicles, On-Demand Mobility, and Environmental Impacts. *Current Sustainable/Renewable Energy Reports*, *2*(3), 74–81. https://doi.org/10.1007/s40518-015-0038-5

Gu, Y., Hsu, L. T., & Kamijo, S. (2016). GNSS/Onboard Inertial Sensor Integration with the Aid of 3-D Building Map for Lane-Level Vehicle Self-Localization in Urban Canyon. *IEEE Transactions on Vehicular Technology*, *65*(6), 4274–4287. https://doi.org/10.1109/TVT.2015.2497001

Helala, M. A., Pu, K. Q., & Qureshi, F. Z. (2012). Road boundary detection in challenging scenarios. In *Proceedings—2012 IEEE 9th International Conference on Advanced Video and Signal-Based Surveillance, AVSS 2012*, 428–433. https://doi.org/10.1109/AVSS.2012.61

Hoang, T. M., Hong, H. G., Vokhidov, H., & Park, K. R. (2016). Road Lane Detection by Discriminating Dashed and Solid Road Lanes Using a Visible Light Camera Sensor. *Sensors, 16*(8), 1313. https://doi.org/10.3390/S16081313

Horani, M., & Rawashdeh, O. (2019). A framework for vision-based lane line detection in adverse weather conditions using vehicle-to-infrastructure (V2I) communication. *SAE Technical Papers*, *2019-April*. https://doi.org/10.4271/2019-01-0684

Ilas, C. (2013). Electronic sensing technologies for autonomous ground vehicles: A review. *2013 8th International Symposium on Advanced Topics in Electrical Engineering (ATEE)*, 1–6. https://doi.org/10.1109/ATEE.2013.6563528

Janai, J., Güney, F., Behl, A., & Geiger, A. (2020). Computer Vision for Autonomous Vehicles: Problems, Datasets and State of the Art. *Foundations and Trends® in Computer Graphics and Vision*, *12*(1–3), 1–308. https://doi.org/10.1561/0600000079

Jiang, T. X., Huang, T. Z., Zhao, X. Le, Deng, L. J., & Wang, Y. (2019). FastDeRain: A Novel Video Rain Streak Removal Method Using Directional Gradient Priors. *IEEE Transactions on Image Processing*, *28*(4), 2089–2102. https://doi.org/10.1109/TIP.2018.2880512

Kalra, N., & Paddock, S. M. (2016). Driving to safety: How many miles of driving would it take to demonstrate autonomous vehicle reliability? *Transportation Research Part A: Policy and Practice*, *94*, 182–193. https://doi.org/10.1016/j.tra.2016.09.010

Khan, H. U., Ali, A. R., Hassan, A., Ali, A., Kazmi, W., & Zaheer, A. (2020). *Lane detection using lane boundary marker network with road geometry constraints* (pp. 1834–1843).

Kim, B., Lee, S., Kim, K., Yoon, J. W., & Han, S.-H. (2015). Pulse-induction metal detector with time-domain bucking circuit for landmine detection. *Electronics Letters*, *51*(2), 159–161. https://doi.org/10.1049/el.2014.3895

Liu, Y. F., Jaw, D. W., Huang, S. C., & Hwang, J. N. (2018). DesnowNet: Context-Aware Deep Network for Snow Removal. *IEEE Transactions on Image Processing*, *27*(6), 3064–3073.

https://doi.org/10.1109/TIP.2018.2806202

Medek, R., Nicolics, J., & Schrottmayer, D. (2001). High sensitive pulse inductive eddy current measurement for mine detection systems. In *24th International Spring Seminar on Electronics Technology. Concurrent Engineering in Electronic Packaging. ISSE 2001. Conference Proceedings* (Cat. No.01EX492), 207–211. https://doi.org/10.1109/ISSE.2001.931058

Milanés, V., Naranjo, J. E., González, C., Alonso, J., & de Pedro, T. (2008). Autonomous vehicle based in cooperative GPS and inertial systems. *Robotica*, *26*(5), 627–633. https://doi.org/10.1017/S0263574708004232

Moreland, C. (2002). Fluxgate Magnetometer. *ReVision*, 1–9. https://www.geotech1.com/pages/mag/projects/fmx1/fmx1.pdf

Moreno-Navarro, F., Iglesias, G. R., & Rubio-Gámez, M. C. (2019). Encoded asphalt materials for the guidance of autonomous vehicles. *Automation in Construction*, *99*, 109–113. https://doi.org/10.1016/J.AUTCON.2018.12.004

Overton, G., & Moreland, C. (2012). *Inside the Metal Detector*. Geotech Press.

Pan, X., Shi, J., Luo, P., Wang, X., & Tang, X. (2018.). Spatial as deep: Spatial cnn for traffic scene understanding. In *Thirty-Second AAAI Conference on Artificial Intelligence.* Retrieved September 16, 2021, from https://www.aaai.org/ocs/index.php/AAAI/AAAI18/paper/download/16802/16322

Primdahl, F. (1979). The fluxgate magnetometer. *Journal of Physics E: Scientific Instruments,* 12(4), 241. https://doi.org/10.1088/0022-3735/12/4/001

Primdahl, F. (1970). The Fluxgate Mechanism, Part I: The Gating Curves of Parallel and Orthogonal Fluxgates. *IEEE Transactions on Magnetics*, 6(2), 376-383. https://doi.org/10.1109/TMAG.1970.1066795

Ren, D., Zuo, W., Hu, Q., Zhu, P., & Meng, D. (2019). *Progressive Image Deraining Networks: A Better and Simpler Baseline,* 3937–3946. https://github.com/csdwren/PReNet.

Ripka, P. (1992). Review of fluxgate sensors. *Sensors and Actuators: A. Physical*, 33(3), 129-141. https://doi.org/10.1016/0924-4247(92)80159-Z

Ripka, P. (2003). Advances in fluxgate sensors. *Sensors and Actuators A: Physical*, *106*(1-3), 8-14.

Rodríguez-Pérez, J. R., Álvarez, M. F., & Sanz-Ablanedo, E. (2007). Assessment of Low-Cost GPS Receiver Accuracy and Precision in Forest Environments. *Journal of Surveying Engineering*, *133*(4), 159–167. https://doi.org/10.1061/(ASCE)0733-9453(2007)133:4(159)

Roesler, J., Bordelon, A., Brand, A., & Amirkhanian, A. (2019). *Fiber-Reinforced Concrete for Pavement Overlays: Technical Overview Final Report*. www.intrans.iastate.edu

Schreiber, M., Knoppel, C., & Franke, U. (2013). LaneLoc: Lane marking based localization using highly accurate maps. In *2013 IEEE Intelligent Vehicles Symposium (IV)*, 449–454. https://doi.org/10.1109/IVS.2013.6629509

Skog, I., & Handel, P. (2009). In-Car Positioning and Navigation Technologies—A Survey. *IEEE Transactions on Intelligent Transportation Systems*, *10*(1), 4–21.

https://doi.org/10.1109/TITS.2008.2011712

Taiebat, M., Brown, A. L., Safford, H. R., Qu, S., & Xu, M. (2018). A Review on Energy, Environmental, and Sustainability Implications of Connected and Automated Vehicles. *Environmental Science & Technology, 52(20), 11449-11465*. https://doi.org/10.1021/acs.est.8b00127

Tao, Z., Bonnifait, P., Fremont, V., & Ibanez-Guzman, J. (2013a). Lane marking aided vehicle localization. In *16th International IEEE Conference on Intelligent Transportation Systems (ITSC 2013)*, 1509–1515. https://doi.org/10.1109/ITSC.2013.6728444

Tao, Z., Bonnifait, P., Fremont, V., & Ibanez-Guzman, J. (2013b). Mapping and localization using GPS, lane markings and proprioceptive sensors. In *2013 IEEE/RSJ International Conference on Intelligent Robots and Systems*, 406–412. https://doi.org/10.1109/IROS.2013.6696383

You, Z. (2018). Chapter 9 - Magnetometer Technology. In *Micro and Nano Technologies,* 341–360. Butterworth-Heinemann. https://doi.org/10.1016/B978-0-12-812672-1.00009-6

Zhu, H., Yuen, K. V., Mihaylova, L., & Leung, H. (2017). Overview of Environment Perception for Intelligent Vehicles. *IEEE Transactions on Intelligent Transportation Systems*, *18*(10), 2584–2601. https://doi.org/10.1109/TITS.2017.2658662